Commun. Comput. Phys.
doi: 10.4208/cicp.090413.130913s

Vol. **15**, No. 4, pp. 895-910
April 2014

Radar Cross Section Reduction of a Cavity in the Ground Plane

Gang Bao[1,2,*] and Jun Lai[2]

[1] *Department of Mathematics, Zhejiang University, Hangzhou 310027, Zhejiang, China.*
[2] *Department of Mathematics, Michigan State University, East Lansing, MI 48824, USA.*

Received 9 April 2013; Accepted (in revised version) 13 September 2013

Available online 21 January 2014

Abstract. This paper investigates the reduction of backscatter radar cross section (RCS) for a rectangular cavity embedded in the ground plane. The bottom of the cavity is coated by a thin, multilayered radar absorbing material (RAM) with possibly different permittivities. The objective is to minimize the backscatter RCS by the incidence of a plane wave over a single or a set of incident angles. By formulating the scattering problem as a Helmholtz equation with artificial boundary condition, the gradient with respect to the material permittivities is determined efficiently by the adjoint state method, which is integrated into a nonlinear optimization scheme. Numerical example shows the RCS may be significantly reduced.

AMS subject classifications: 35Q93, 35J05

Key words: Optimal design, RCS reduction, adjoint method, radar absorbing materials.

1 Introduction

Radar cross section (RCS) is an important measure for the detection of a target by radar systems. The RCS from a cavity is significant since the overall RCS of a target is often dominated by some cavities, such as the jet inlet of an aircraft. Therefore, effective reduction of the RCS from a cavity has been an important problem in wave propagation with many practical applications. In this paper, we focus on a 2-D rectangular cavity which is embedded in the ground plane and illuminated by a time-harmonic plane wave. A thin, multilayered RAM is coated horizontally at the bottom of the cavity for the reduction of backscatter RCS, as shown in Fig. 1.

*Corresponding author. *Email addresses:* bao@math.msu.edu (G. Bao), laijun@msu.edu (J. Lai)

Many methods have been proposed on RCS reduction with RAM [7,15,17]. A popular one is based on genetic algorithm (GA), which is a gradient-free optimization method and widely used in engineering community. The problem is, even for a small parameter space, GA usually requires thousands of generations to obtain the best population, or the global optimal. While designing a fast algorithm for the direct scattering problem already presents a huge challenge especially when the cavity is large and deep [10,13], it is computationally unaffordable to employ GA to find the optimal synthesized RAM of a cavity.

In this paper, the problem is addressed by the gradient-based sequential quadratic programming (SQP) method. SQP is a one of the most effective optimization methods particularly for nonlinear constraint like partial differential equations (PDE) [16]. The basic idea of this method is to generate steps by solving a sequence of quadratic subproblems. The gradient involved in the quadratic subproblems is provided accurately by the continuous adjoint state method. The accuracy plays an important role in the design especially when the backscatter RCS is highly sensitive to the change of permittivities.

Due to the difficulty in the forward scattering problem of a cavity as we mentioned, a crucial step underlying the optimization method is to find a fast solver for the direct problem. Lots of methods have been studied during the last decades. Standard techniques include method of moment (MoM) [9] or the finite element-boundary integral (FE-BI) method [10]. High frequency asymptotic approaches include Gaussian beam shooting [6], the bounding and shooting ray method [12]. Recently, we also proposed a fast mode matching method for 2-D and 3-D large cavities [3,5]. Mathematical analysis for the cavity scattering problem can be seen in [1, 2]. In order to satisfy both the efficiency and the accuracy, we adopt the method proposed in [4], which is based on finite difference with second order accuracy in the interior.

In the following section, the optimal design of a cavity with multilayered RAM is formulated as a minimization problem, with the constraint being formulated as a Helmholtz equation with artificial boundary condition. The objective function and design variables are also defined in this section. The continuous adjoint method is applied in Section 3 for the gradient of the backscatter RCS. Section 4 introduces the SQP optimization technique to the RCS reduction. Numerical experiments are provided in Section 5 to show the application of the method.

2 Problem formulation

Consider a rectangular cavity $\Omega=[0,a]\times[-b,0]$ embedded in a ground plane illuminated by a plane wave, as illustrated in Fig. 1. The problem is in 2-D by assuming the cavity and the materials are invariant in the z direction. Above the ground plane is empty space with dielectric permittivity ε_0. The surface of the ground plane Γ^c and the boundary S of the cavity are assumed to be perfect conductors. The cavity is filled with inhomogeneous material in layered structure with permittivities ε_i, $i=1,2,\cdots,n$, where n is the number

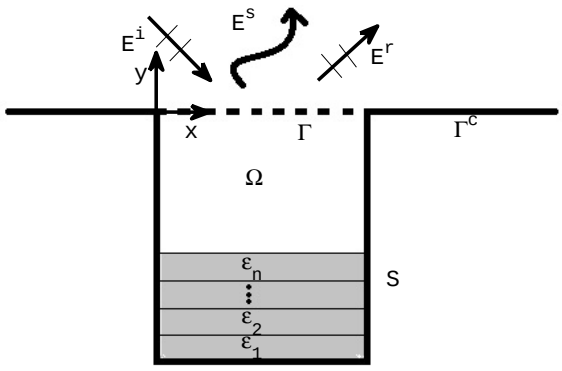

Figure 1: Geometry of the problem.

of layers and presumably small from the practical point of view. Assume the magnetic permeability μ_0 is the same everywhere.

In 2-D, there are two fundamental polarizations in the wave propagation, namely, TM (transverse magnetic) polarization and TE (transverse electric) polarization. In this paper, we consider TM polarization only, which implies the magnetic field is transverse to the xy plane and the electrical field is simply expressed as $(0,0,u(x,y))$. The goal is to determine the permittivities of the coating material within a small thickness h such that the backscatter RCS is minimized.

Assume the incident field is given by a plane wave: $u^i = e^{j(\alpha x-\beta y)}$, where $\alpha = k_0\cos\theta$, $\beta = k_0\sin\theta$, θ is the incident angle with respect to the x-axis. Let $k = \omega\sqrt{\varepsilon\mu_0}$ be the wavenumber in the space. In particular, $k_0 = \omega\sqrt{\varepsilon_0\mu_0}$ is the wavenumber in the upper half space $\mathbb{R}^{2+}$. Denote $u(x,y)$ and $u^s(x,y)$ as the total electrical field and the scattered field respectively. The total field $u(x,y)$ can be expressed as :

$$u(x,y) = u^s(x,y) + u^i - e^{j(\alpha x+\beta y)}, \tag{2.1}$$

where $-e^{j(\alpha x+\beta y)}$ is identified as the reflected field u^r caused by the infinite ground plane. In addition, $u(x,y)$ satisfies the following equation:

$$\Delta u + k^2 u = 0 \qquad \text{in } \Omega\cup\mathbb{R}^{2+}, \tag{2.2a}$$

$$u = 0 \qquad \text{on } \Gamma^c\cup S, \tag{2.2b}$$

together with the radiation condition satisfied by u^s:

$$\lim_{\rho\to\infty}\rho^{1/2}\Big(\frac{\partial u^s}{\partial\rho} - ik_0u^s\Big) = 0, \tag{2.3}$$

where $\rho = \sqrt{x^2+y^2}$.

In general, analyzing Eq. (2.2) directly is difficult both theoretically and numerically due to the unboundedness of the domain. The general approach is to introduce some

kind of artificial boundaries so that the domain is reduced to be bounded. Here we introduce a transparent boundary condition, which essentially is *Dirichlet-to-Neumann* (DtN) map, to truncate the unbounded domain. The idea of transparent boundary condition has been applied to many wave scattering problems; for instance, see [14]. Following the formulation in [1], we derive the boundary condition based on the Fourier Transform.

The exterior scattered field $u^s(x,y)$ satisfies the equation:

$$\Delta u^s + k_0^2 u^s = 0 \quad \text{in } \mathbb{R}^{2+}, \tag{2.4a}$$

$$u^s = \psi(x,0) \quad \text{on } \Gamma, \tag{2.4b}$$

$$u^s = 0 \quad \text{on } \Gamma^c, \tag{2.4c}$$

together with the radiation condition (2.3). Here we assume $\psi(x,0)$ is the known scattered field at the aperture Γ.

Take the Fourier Transform of u^s with respect to variable x and denote it by $\widehat{u^s}(\xi,y)$. Eq. (2.4) becomes:

$$\frac{\partial^2 \widehat{u^s}}{\partial y^2} + (k_0^2 - \xi^2)\widehat{u^s} = 0, \tag{2.5a}$$

$$\widehat{u^s}(\xi,0) = \widehat{\widetilde{\psi}}(\xi,0) \quad \text{on } \Gamma \cup \Gamma^c, \tag{2.5b}$$

where $\widetilde{\psi}(x,0)$ denotes the zero extension of $\psi(x,0)$ on $y=0$. This equation admits a simple solution:

$$\widehat{u^s}(\xi,y) = \widehat{\widetilde{\psi}}(\xi,0) e^{i\sqrt{k_0^2-\xi^2}y}. \tag{2.6}$$

We drop another linearly independent solution by the radiation condition (2.3). Taking an inverse Fourier Transform of (2.6) yields the following solution for u^s:

$$u^s(x,y) = \frac{1}{2\pi}\int_{\mathbb{R}} \widehat{\widetilde{\psi}}(\xi,0) e^{i\sqrt{k_0^2-\xi^2}y} e^{i\xi x} d\xi. \tag{2.7}$$

Differentiating both sides with respect to y at $y=0$ gives us:

$$\frac{\partial u^s}{\partial n}\Big|_{y=0^+} = \frac{i}{2\pi}\int_{\mathbb{R}} \sqrt{k_0^2-\xi^2}\,\widehat{\widetilde{\psi}}(\xi,0) e^{i\xi x} d\xi. \tag{2.8}$$

We use $y=0^+$ since the derivative is derived from $y>0$. From the expression (2.1) for the total field u and the fact $u^i + u^r = 0$ on $y=0$, it yields:

$$\frac{\partial u}{\partial n}\Big|_{y=0^+} = I(u) + g, \tag{2.9}$$

where $g = 2i\beta e^{i\alpha x}$ and $I(\cdot)$ is the boundary operator defined by:

$$I(u) = \frac{i}{2\pi}\int_{\mathbb{R}} \sqrt{k_0^2-\xi^2}\,\widehat{u}(x,0) e^{i\xi x} d\xi. \tag{2.10}$$

By the continuity condition on the boundary Γ, boundary condition (2.9) is also satisfied by u in Ω. We therefore reduce the unbounded domain problem for u to the following:

$$\Delta u+k^2u=0 \qquad \text{in } \Omega, \tag{2.11a}$$

$$u=0 \qquad \text{on } S, \tag{2.11b}$$

$$\frac{\partial u}{\partial n}=I(u)+g(x) \qquad \text{on } \Gamma. \tag{2.11c}$$

Problem (2.11) is uniquely solvable for any incident plane wave. Proof can be found in [1].

2.1 Objective function

The RCS reduction problem may be formulated as minimizing the following cost function:

$$\sigma:=\frac{4}{k_0}\left|\frac{k_0}{2}\sin\theta\int_\Gamma ue^{-jk_0x\cos\theta}dx\right|^2, \tag{2.12}$$

which is the backscatter RCS for TM polarization [11]. In the case of the RCS reduction over a set of incident angles $\{\theta_1,\theta_2,\cdots,\theta_m\}$, the cost function may be changed to the following:

$$\sigma_t:=\sum_{l=1}^{m}w_l\sigma(\theta_l), \tag{2.13}$$

where $w_l>0$, $l=1,2,\cdots,m$ are the weights for different angles. Furthermore, depending on which angle is important, these weights may be chosen accordingly.

Since u depends on ε from the model (2.11), the optimization problem can be rewritten as:

$$\min_{\varepsilon\in\Lambda}\sigma(\varepsilon), \tag{2.14}$$

where the admissible set Λ for electrical permittivity ε satisfies the following two conditions:

- *Layered medium:* $\varepsilon(y)$ in Λ is constant for each layer, either lossy or lossless. In other words, $\varepsilon(y)=\varepsilon_j$ at the jth layer, where $\varepsilon_j=\varepsilon_j'+i\varepsilon_j''$, $j=1,2,\cdots,n$, n is the number of layers of the coating material. In particular, permittivity with nonzero imaginary part corresponds to lossy material.
- *Boundness:* We assume there exist two constants $\varepsilon_{\min}=\varepsilon'_{\min}+i\varepsilon''_{\min}$ and $\varepsilon_{\max}=\varepsilon'_{\max}+i\varepsilon''_{\max}$ such that $\varepsilon'_{\min}<\varepsilon_j'<\varepsilon'_{\max}$ and $\varepsilon''_{\min}<\varepsilon_j''<\varepsilon''_{\max}$ for $j=1,2,\cdots,n$. Namely, the permittivity $\varepsilon(y)$ is bounded between $\varepsilon_{\min}$ and $\varepsilon_{\max}$.

The existence of the minimizer for (2.14) follows from the compactness of the admissible set Λ and the continuous dependence of the total field u on the permittivity ε, but the uniqueness of the minimizer generally does not hold. To investigate the concavity of the

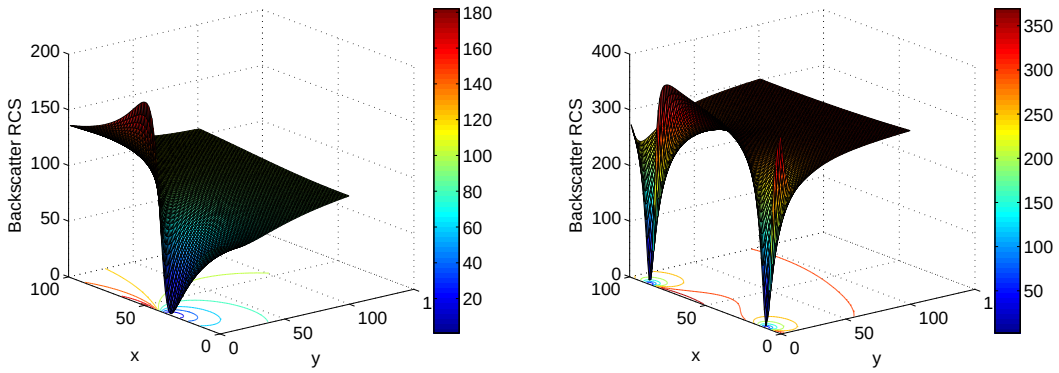

(a) (b)

Figure 2: Backscatter RCS at normal incidence with one-layer coating. X axis is the real part of the relative permittivity ε for the coating material. Y axis is the corresponding imaginary part. (a) When $k_0=16\pi$, a local minimum is located at $[33.491,0]$ with RCS 0.56. (b) When $k_0=32\pi$, two local minimums exist. One is located at $[10.739,0]$ with RCS 0.727, and another one is located at $[87.517,0]$ with RCS 0.732.

optimization problem (2.14), we simply consider a one-layer coating problem. Assume the dimension of the cavity is $[0,1]\times[-0.3,0]$. The thickness of the coating layer is 0.0047. Figs. 2(a), (b) show the backscatter RCS at the normal incidence for $k_0=16\pi$ and $k_0=32\pi$, respectively.

From Fig. 2, we observe two facts: the first is in general the optimization problem (2.14) is not concave, so our gradient based method is only expected to generate a local minimum; the second is in a given region, higher wavenumber tends to generate more local minimums, which increases the difficulty for optimal design in the high frequency. However, one good thing is that the value of those local minimums are very close to each other. Hence, although we do not expect to find a global minimum, we expect to find a very reasonable local minimum using the gradient based method. We therefore proceed to discuss how to find the gradient of the objective function efficiently in the next section.

3 Gradient by the adjoint state method

To use a gradient based optimization method for the backscatter RCS (2.12) with respect to the permittivity, we need to evaluate the gradient along with the PDE constraint (2.11). Here we adopt the adjoint state method to give the gradient for TM polarization. The adjoint state method has a broad range of applications in nonlinear optimizations; see [8] for example. Theoretically, the gradient obtained by the adjoint state method is more accurate compared to the approximated gradient given by the finite difference. Numerically, it is also more efficient since the evaluation only requires solving an extra adjoint problem regardless of the number of variables. Here we give a formal derivation of the gradient.

Denote the far field coefficient:

$$P_\theta(\varepsilon)=\frac{k_0}{2}\sin\theta\int_\Gamma ue^{-ik_0x\cos\theta}dx. \tag{3.1}$$

Then

$$\sigma(\varepsilon)=\frac{4}{k_0}|P_\theta(\varepsilon)|^2.$$

Let $\delta\varepsilon$ be a "small" perturbation to the permittivity ε. We denote the linearization of $\sigma(\varepsilon)$ with respect to $\delta\varepsilon$ by $\delta\sigma$, which is:

$$\delta\sigma=2Re\Big(\frac{4}{k_0}\delta P\overline{P_\theta}(\varepsilon)\Big), \tag{3.2}$$

where δP denotes the linearization of $P_\theta(\varepsilon)$ and $\overline{P_\theta}$ is the complex conjugate of P_θ. From (3.1), it is easy to calculate that

$$\delta P=\frac{k_0}{2}\sin\theta\int_\Gamma \delta ue^{-ik_0x\cos\theta}dx, \tag{3.3}$$

where δu solves the linearized problem

$$\Delta\delta u+k^2\delta u=-(\omega^2\mu_0\delta\varepsilon)u \qquad \text{in } \Omega, \tag{3.4a}$$
$$\delta u=0 \qquad \text{on } S, \tag{3.4b}$$
$$\frac{\partial\delta u}{\partial n}=I(\delta u) \qquad \text{on } \Gamma. \tag{3.4c}$$

Let u^* solve the adjoint state equation:

$$\Delta u^*+\overline{k^2}u^*=0 \qquad \text{in } \Omega, \tag{3.5a}$$
$$u^*=0 \qquad \text{on } S, \tag{3.5b}$$
$$\frac{\partial u^*}{\partial n}=I^*(u^*)+e^{ik_0x\cos\theta}P_\theta(\varepsilon) \qquad \text{on } \Gamma, \tag{3.5c}$$

where $I^*(u^*)$ is the adjoint operator of $I(u)$, given by

$$I^*(u^*)=\frac{-i}{2\pi}\int_{\mathbb{R}}\overline{\sqrt{k_0^2-\xi^2}}\widehat{\overline{u^*}}(x,0)e^{i\xi x}d\xi.$$

Given Eqs. (3.4) and (3.5), an integration by parts yields that

$$\int_\Omega\omega\mu_0\delta\varepsilon\cdot u\overline{u^*}dx=\int_\Gamma\delta ue^{-ik_0x\cos\theta}ds\cdot\overline{P_\theta(\varepsilon)}. \tag{3.6}$$

Comparing with (3.2), we then have

$$\delta\sigma=4Re\Big(\sin\theta\int_\Omega\omega^2\mu_0\delta\varepsilon\cdot u\overline{u^*}dx\Big). \tag{3.7}$$

Up to a constant multiple, the gradient of the cost function $\sigma(\varepsilon)$ is the function $g(\varepsilon)$ such that

$$\delta\sigma(\varepsilon) = Re\int_{-b}^{0}\delta\varepsilon\overline{g(\varepsilon)}dy. \tag{3.8}$$

Comparing (3.7) with (3.8), we arrive at the formula for the gradient:

$$g(\varepsilon) = 4\sin\theta\omega^2\mu_0\int_0^a \overline{u}u^*dx, \tag{3.9}$$

where u^* is the solution of (3.5).

For the cost function (2.13), since it is a linear combination of (2.12), the gradient can be easily deduced from (3.9). It can be seen that the adjoint problem shares the same structure as the original scattering problem, hence the same solver may be used for the adjoint problem. This is a huge advantage given the level of difficulties for solving the scattering problem from a cavity. In the numerical approximation, the finite-dimensional counterpart of the gradient (3.9) is used, which is given by:

$$\Big(\int_{-b}^{-b+h}\overline{g(\varepsilon)}dy, \int_{-b+h}^{-b+2h}\overline{g(\varepsilon)}dy, \cdots, \int_{-b+(n-1)h}^{-b+nh}\overline{g(\varepsilon)}dy\Big), \tag{3.10}$$

where h is the thickness of each layer. Table 1 gives a comparison between the gradient obtained by (3.10) and the numerical gradient obtained by finite difference. Assume the dimension of the cavity is $[0,1]\times[-0.3,0]$ with two layers of coating material placed at the bottom. The permittivities of the two layers are $(1+i,2+2i)$ with the thickness of each layer being 5.848E-4. Consider the normal incidence of a plane wave with $k_0 = 16\pi$ on the cavity. The ratio between these two gradients are close to one, but the computational time by (3.9) is much smaller than the time spent by the finite difference. The time gap will enlarge as the number of design variables increase. The efficiency and accuracy of the gradient obtained by the adjoint state method provide a huge advantage for the optimization method.

Table 1: A comparison for the gradients obtained from the adjoint state method (ASM) and the finite difference method (FDM).

	$Re(\varepsilon_1)$	$Im(\varepsilon_1)$	$Re(\varepsilon_2)$	$Im(\varepsilon_2)$	CPU Time
ASM	-8.8402E-6	-3.2758E-5	-3.8514E-4	-1.5E-3	2.24s
FDM	-8.8332E-6	-3.2730E-5	-3.8514E-4	-1.5E-3	3.89s
Ratio	1.0008	1.0008	1.0000	1.0000	

4 Optimization method: sequential quadratic programming

We adopt the Sequential Quadratic Programming (SQP) method to optimize the problem (2.14) largely because of its outstanding performance on the nonlinear constraint problem. For a sufficiently smooth problem, this method provides a superlinear convergence

near the region of optimal point under some suitable assumptions [16]. The principle idea is to generate a sequence of quadratic programming (QP) subproblems that are based on the approximation of Lagrangian function in a small region. For each QP subproblem, the solution is used to form a search direction for a line search. In general the Hessian matrix used in the QP subproblem is not obtained analytically, but instead is updated by some quasi-Newton methods. Here we give three steps on how to apply SQP to our problem. One resorts to [16] for a complete discussion on this method.

Step 1: Let $d=(Re(\varepsilon_1),Im(\varepsilon_1),Re(\varepsilon_2),\cdots,Im(\varepsilon_n))^T=(d_i)_{j=1}^{j=2n}$. Define a sequence of functions $\{h_j(d)\}_{j=1}^{j=4n}$ to be:

$$\begin{aligned} h_{4(j-1)+1}(d)&=d_{2j-1}-\varepsilon'_{\max}, \qquad & h_{4(j-1)+2}(d)&=\varepsilon'_{\min}-d_{2j},\\ h_{4(j-1)+3}(d)&=d_{2j-1}-\varepsilon''_{\max}, \qquad & h_{4(j-1)+4}(d)&=\varepsilon''_{\min}-d_{2j}, \end{aligned}$$

for $j=1,2,\cdots,n$. It is easily seen that $h_j(\varepsilon)\leq 0$ means ε is bounded below and above by the two constants $\varepsilon_{\min}$ and $\varepsilon_{\max}$. Hence, Problem (2.14) can be rewritten in the following form:

$$\begin{aligned} &\min_{d\in\mathbb{R}^{2n}} \sigma(d) \\ &\text{subject to } \ h_j(d)\leq 0, \quad \text{for } \ j=1,2,\cdots,4n. \end{aligned} \tag{4.1}$$

Define the Lagrangian function for (4.1):

$$L(d,\lambda)=\sigma(d)+\sum_{j=1}^{4n}\lambda_j h_j(d), \tag{4.2}$$

where λ_j is the Lagrangian multiplier.

Step 2: It is difficult to solve (4.2) directly due to the nonlinearity of $\sigma(d)$. The idea is to replace (4.2) by its quadratic approximation, which results in a QP subproblem, so that many QP algorithms can be used. At the $m-$th iteration, the QP subproblem of SQP when $d=d^{(m)}$ is given by:

$$\begin{aligned} &\min_{x\in\mathbb{R}^{2n}} g(d^{(m)})^T x+\frac{1}{2}x^T H_m x \\ &\text{subject to } \ h_j(d^{(m)}+x)\leq 0, \quad \text{for } \ j=1,2,\cdots,4n, \end{aligned} \tag{4.3}$$

where $g(d^{(m)})$ is the gradient of $\sigma(d)$ at $d^{(m)}$ and H_m is the Hessian of the Lagrangian function (4.2), which is in fact the Hessian of $\sigma(d)$ by the linearity of the constraint. It is usually approximated by some quasi-Newton methods to keep the Hessian positive definite. Here we choose the widely used Broyden-Fletcher-Goldfarb-Shanno (BFGS) formula, which is given by:

$$H_{m+1}=H_m-\frac{H_m^T x_m^T x_m H_m}{x_m^T H_m x_m}+\frac{y_m y_m^T}{y_m^T x_m}, \tag{4.4}$$

where

$$x_m = d^{(m+1)} - d^{(m)}, \tag{4.5a}$$

$$y_m = g(d^{(m+1)}) - g(d^{(m)}). \tag{4.5b}$$

The Hessian keeps being positive definite whenever the initial Hessian matrix H_0 is positive definite and $y_m^T x_m > 0$. This follows from the following identity:

$$z^T H_{m+1} z = (z-\omega)^T H_m (z-\omega) + \frac{z^T y_m y_m^T z}{y_m^T x_m}, \tag{4.6}$$

where $\omega = x_m x_m^T H_m z / x_m^T H_m x_m$ and z is an arbitrary vector in $\mathbb{R}^{2n}$. Issues can happen when $y_m^T x_m < 0$. In that case we modify y_m component-wise such that $y_m^T x_m > 0$ is satisfied.

Step 3: The solution of the subproblem (4.3) yields a new step:

$$d^{(m+1)} = d^{(m)} + \alpha x. \tag{4.7}$$

The step length $\alpha \in (0,1)$ can be determined by an appropriate defined merit function. Here we use the following L^1 merit function:

$$\varphi(\varepsilon) = \sigma(\varepsilon) + \sum_j^{4n} \mu_j \max(0, h_j(\varepsilon)) \tag{4.8}$$

for sufficiently large μ_j.

We are now ready to state the minimization algorithm:

1. Given the convergence tolerance $\epsilon > 0$, the initial value $d^{(0)}$ and $H_0 = I$, where I is the identity matrix, and $m = 0$.
2. Repeat, until $\|x\| < \epsilon$
   - Evaluate $g(d^{(m)})$, H_m;
   - Solve (4.3) to obtain x;
   - Set $d^{(m+1)} = d^{(m)} + \alpha x$,

   where α is determined by the merit function (4.8).
   End

Note that the solution obtained by this way is by no means the global minimum. What we expect is only local minimum. Depending on different applications, we either expect there is a good initial value available or try different initial values in the admissible set and choose the most "optimal" one after running the optimization.

5 Direct solver for the forward scattering problem

Numerical solution of the electromagnetic scattering from a cavity has been known as a challenging problem for decades [13], especially when the size of the cavity is big or the wavenumber is large. Here we choose the finite difference algorithm developed in [4] as the direct solver. The general idea of the algorithm is presented in this section with details referred to [4].

Assume the domain Ω is uniformly partitioned by $\{x_i,y_j\}_{i,j}^{M+1,N+1}$ with $x_{j+1}-x_j=h_x, y_{j+1}-y_j=h_y$. Let u_{ij} denote the numerical approximation at (x_i,y_j). The second order finite difference scheme to the Helmholtz equation (2.11) is given by:

$$\frac{u_{i+1,j}-2u_{i,j}+u_{i-1,j}}{h_x^2}-\frac{u_{i,j+1}-2u_{i,j}+u_{i,j+1}}{h_y^2}+k^2(y_j)u_{i,j}=0,$$
$$i=1,2,\cdots,M;\quad j=1,2,\cdots,N. \tag{5.1}$$

By Green's function method, the transparent boundary operator can be reformulated as:

$$I(u)=-\frac{k_0}{2j}\oint\!\!\!\!\!\!-_{\Gamma}\frac{1}{|\mathbf{x}-\mathbf{x}'|}H_1^{(1)}(k_0|x-x'|)u(x',0)dx', \tag{5.2}$$

where $\oint\!\!\!\!\!\!-\cdot dx$ denotes the Hadamard principal value (or finite part) integral and $H_1^{(1)}(\cdot)$ is the first order Hankel's function of the first kind. After the reformulation, we apply the first order numerical approximation for the transparent boundary condition:

$$\frac{u_{i,N+1}-u_{i,N}}{h_y}=\sum_{i=1}^{M}w_iu_{i,N+1}+g(x_i),\quad i=1,2,\cdots,M, \tag{5.3}$$

where the weights w_i for the hypersingular integral (5.2) can be evaluated efficiently through the method proposed by Sun et al. in [18]. The idea of the algorithm in [4] is to use the discrete sine transform in the horizontal direction and a Gaussian elimination in the vertical direction. The resulting system becomes an $M\times M$ linear system, which is much smaller than the original one. It then can be solved by any linear solver with an appropriate preconditioner. Since the algorithm highly utilizes the special structure of the cavity problem, it is extremely fast and efficient, which fits exactly into the requirement for a computation engine of the optimization method.

6 Numerical experiments

In this section, we apply our algorithm to the RAM design through three numerical examples. The goal is to show that RCS can be reduced with appropriate coating material inside the cavity. Throughout, we assume the dimension of cavity is $1m$ in width and $0.3m$ in depth. The cavity is uniformly partitioned by a 512×512 mesh. The thickness

of the coating material for each layer is $0.6mm$, up to 8 layers. For each layer, the initial value of the relative permittivity is set to be $5+5i$, and assume it can be continuously changing between $1+0i$ and $100+100i$. The artificial material is used only for illustration purpose. All the computation is carried out on a laptop with Intel dual core 2.1Ghz and memory 4GB. For physical interest, the RCS is expressed in terms of decibel(dB), which is

$$\text{RCS: } = 10\log_{10}\sigma\text{dB}.$$

Example 6.1. Consider the scattering from the cavity by the incidence of a plane wave with wavenumber $k_0 = 16\pi$. Fig. 3(a) gives the result for the optimization at normal incidence. RCS are reduced by more than 20dB at $\theta = \pi/2$. However, the reduction immediately disappears after $\theta = \pi/2$ and starts to oscillate. The overall effect of the coating material is very limited. Fig. 3(b) shows the result for RCS optimization at $\theta = 3\pi/5$. The deep well in the graph shows a large amount of reduction at $\theta = 3\pi/5$. Unlike the optimization at $\theta = \pi/2$, the RCS reduction is not only confined around $\theta = 3\pi/5$. It also extends to the other angular sector with an average reduction around 10dB, which can be considered as a large improvement. Similar effect has been shown in Fig. 3(c), which gives the RCS when the optimization is conducted at $\theta = 5\pi/6$. As expected, large amount of reduction appears at $\theta = 5\pi/6$. Meanwhile, the RCS at the other angular sector also gets reduced. The resulted relative permittivities are listed in Table 2 with the corresponding number of iterations and CPU time.

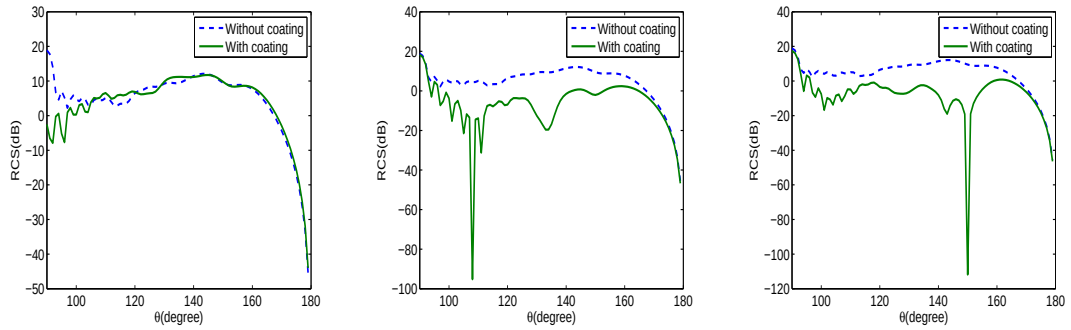

Figure 3: RCS reduction for $k_0 = 16\pi$. (a) Optimized at $\theta = \pi/2$. (b) Optimized at $\theta = 3\pi/5$. (c) Optimized at $\theta = 5\pi/6$.

Example 6.2. Consider the incidence of a plane wave with wavenumber $k_0 = 32\pi$ on the cavity. The optimization are performed at $\theta = \pi/2, 3\pi/5, 5\pi/6$ as the last example. Fig. 4(a) gives the result for the optimization at normal incidence. RCS are reduced by more than 25dB at $\theta = \pi/2$. However, similar to Example 6.1, the reduction appears only in a small interval around $\theta = \pi/2$ and tend to disappear beyond $\theta = 5\pi/9$. Fig. 4(b) shows the result for RCS optimization at $\theta = 3\pi/5$. The deep well in the graph shows

Table 2: Relative permittivities after the optimization, number of iterations and CPU time for all the three examples.

	Example 6.1			Example 6.2			Example 6.3	
k_0	16π	16π	16π	32π	32π	32π	16π	32π
θ	$\frac{\pi}{2}$	$\frac{3\pi}{5}$	$\frac{5\pi}{6}$	$\frac{\pi}{2}$	$\frac{3\pi}{5}$	$\frac{5\pi}{6}$	$\frac{3\pi}{5}$, $\frac{5\pi}{6}$	$\frac{3\pi}{5}$, $\frac{5\pi}{6}$
1st(Re)	7.833	11.573	11.516	1	10.588	10.542	35.945	13.985
1st(Im)	0	6.264	6.251	0	6.431	6.283	14.955	40.326
2nd(Re)	1	13.212	12.987	1	9.329	9.162	100	59.028
2nd(Im)	0	9.486	9.432	0	10.143	9.563	32.156	100
3rd(Re)	1	12.980	12.488	1	4.457	4.169	100	1
3rd(Im)	0	4.379	4.242	0	5.722	4.461	13.013	0
4th(Re)	1	22.289	21.434	1	7.485	7.133	100	1
4th(Im)	0	6.270	5.966	0	8.257	6.088	0	0
5th(Re)	1	28.256	26.953	1	5.863	5.653	92.566	1
5th(Im)	0	5.011	4.363	0	7.032	3.844	0	0
6th(Re)	1	43.940	42.115	1	12.887	13.136	1	1
6th(Im)	0	5.473	4.147	0	5.986	1.784	0	0
7th(Re)	31.709	49.497	47.164	1	9.514	10.602	1	1
7th(Im)	0	5.570	2.994	0	1.904	0	0	0
8th(Re)	93.465	62.494	59.890	37.788	13.725	15.910	1	37.949
8th(Im)	0	9.834	4.880	0	1.800	0	0	0
Iter.	115	34	28	107	15	13	198	177
CPU	366.8s	113.2s	150.3s	299.4s	59.3s	59.7s	2065s	1816s

a large amount of reduction at $\theta = 3\pi/5$. The RCS reduction is not only limited around $\theta = 3\pi/5$. It also extends to the other angular sector with an average reduction around 10dB. Fig. 4(c) gives the optimized RCS when the optimization is conducted at $\theta = 5\pi/6$. As expected, a large amount of reduction appears at $\theta = 5\pi/6$. Meanwhile, the RCS at the other angular sector also gets reduced. Table 2 shows all the optimization tests are finished in 400s, which implies the efficiency of the algorithm.

The different performances between the optimization at the normal and the other angles are caused by the geometry of the cavity and the way the coating material takes effect. Mathematical analysis for such differences is rather involved, so we only give a possible explanation based on the ray tracing theory [12]. Because of the thin thickness, the absorbing effect of the coating material is not significant. The main reason that RCS gets reduced is because the propagating directions of the reflected rays get changed by the coating material. While the change may not result in reduction for all incident angles, there exist some unchanged angles or even enhanced angles. Therefore, the optimized coating for normal angle may not work for some oblique angles and vice versa. Based

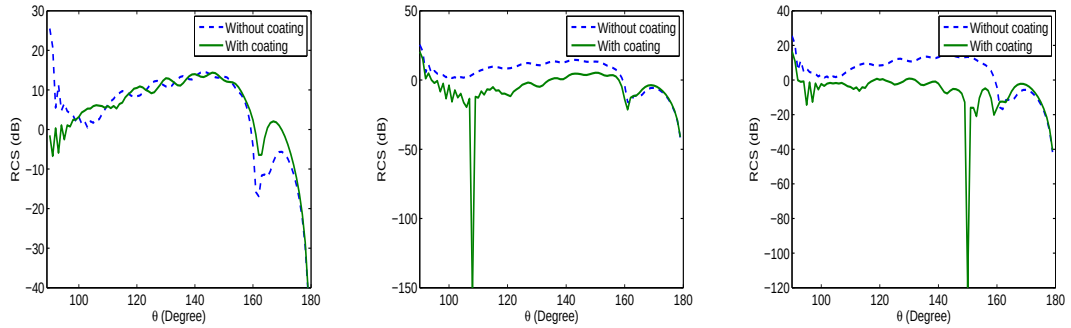

Figure 4: RCS reduction for $k_0=32\pi$. (a) Optimized at $\theta=\pi/2$. (b) Optimized at $\theta=3\pi/5$. (c) Optimized at $\theta=5\pi/6$.

on the observation in the two examples, we conclude wider reduction can be achieved through optimization at the oblique incidence compared to the normal incidence.

Example 6.3. In this example, we try to define the objective function as a combination of RCS at $\theta=3\pi/5$ and $5\pi/6$. The formula is given in (2.13) with equal weights for the two angles. Results are shown in Fig. 5 for both $k_0=16\pi$ and $k_0=32\pi$ and the corresponding CPU time are given in Table 2. The combination of these two angles provides a smoother reduction instead of a sharp decrease at some particular angle. Consequently, it may have more practical applications. Note that it takes much longer time for the method to converge compared to the previous two examples. One obvious reason comes from the fact that the evaluation for the forward problem and the adjoint problem has been doubled. Another reason is because the region around the optimal point is not concave, which slows down the convergence. As we see from Fig. 6, the first few iterations give most of the reduction, while the rest iterations gives very little improvement. Hence, the op-

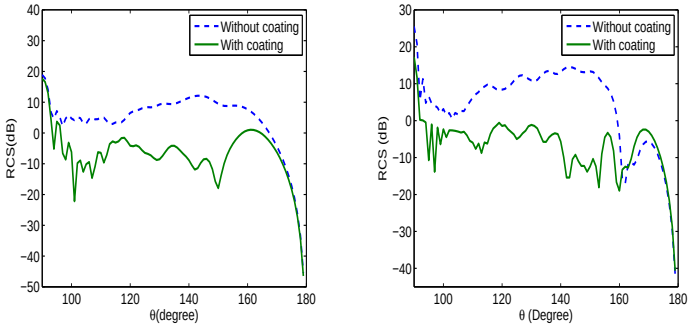

Figure 5: RCS reduction by the combination of $\theta=3\pi/5$ and $\theta=5\pi/6$. (a) Optimized for $k_0=16\pi$. (b) Optimized for $k_0=32\pi$.

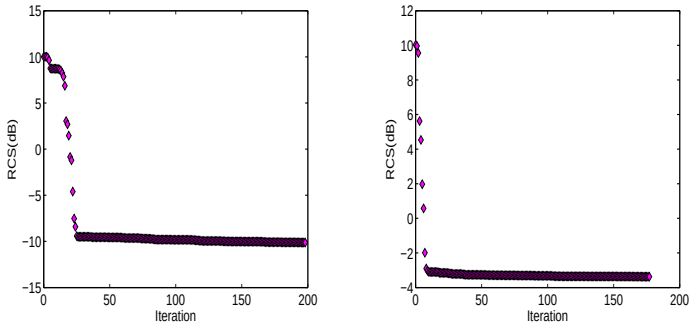

(a) (b)

Figure 6: Convergence of the optimization for RCS reduction by the combination of $\theta=3\pi/5$ and $\theta=5\pi/6$. The solid diamond denotes the sum of RCS at the two angles in each iteration. (a) $k_0=16\pi$. (b) $k_0=32\pi$.

timization can be accelerated by stopping the iteration earlier if no significant reduction appears any more.

7 Conclusions

In this paper, the design of a multilayered RAM for reducing RCS of a cavity is formulated as a minimization problem. The descent direction for the cost function is evaluated through the adjoint state method. Subsequently, SQP is integrated with the gradient to obtain the optimal absorbing materials for the cavity. The algorithm is implemented with a fast and accurate direct solver for the scattering problem. Numerical results show that RCS is reduced significantly with RAM coated at the bottom of the cavity. It is also observed that the optimization at oblique incidence results in a wider RCS reduction compared to the optimization at normal incidence.

Acknowledgments

The research was supported in part by the NSF grants DMS-0908325, DMS-0968360, DMS-1211292, the ONR grant N00014-12-1-0319, a Key Project of the Major Research Plan of NSFC (No. 91130004), and a special research grant from Zhejiang University.

References

[1] H. Ammari, G. Bao and A. W. Wood, Analysis of the electromagnetic scattering from a cavity, Japan J. Indust. Appl. Math., 19 (2002), 301–310.
[2] G. Bao, J. Gao and P. Li, Analysis of direct and inverse cavity scattering problems, Numer. Math. Theor. Meth. Appl., 4 (2011), 419–442.
[3] G. Bao, J. Gao, J. Lin and W. Zhang, Mode matching for the electromagnetic scattering from three-dimensional large cavities, IEEE Trans. Antennas Propagat., 60 (2012), 2004–2010.

[4] G. Bao and W. Sun, A fast algorithm for the electromagmetic scattering from a large cavity, SIAM J. Sci. Comput., 27 (2007), 553–574.
[5] G. Bao and W. Zhang, An improved mode-matching method for large cavities, IEEE Antennas Wireless Propagat. Lett., 27 (2005), 393–396.
[6] R. Burkholder and P. Pathak, Analysis of EM penetration into and scattering by electrically large open waveguide cavities using Gaussian beam shooting, Proc. IEEE, 79 (1991), 1401–1412.
[7] R. Chou and S. Lee, Modal attenuation in multilayered coating waveguide, IEEE Trans. Microwave Theory Tech., 36 (1988), 1167–1176.
[8] D. C. Dobson, Optimal design of periodic antireflective structures for the Helmholtz equation, Euro. J. Appl. Math., 4 (1993), 321–340.
[9] P. Huddleston, Scattering from conducting finite cylinders with thin coatings, IEEE Trans. Antennas Propagat., 35 (1987), 1128–1136.
[10] J. Jin, A finite element-boundary integral formulation for scattering by three-dimensional cavity-backed apertures, IEEE Trans. Antennas Propagat., 39 (1991), 97–104.
[11] J. Jin, The Finite Element Method in Electromagnetics, 2nd ed. New York, Wiley, 2002.
[12] H. Ling, R. Chou, and S. Lee, Shooting and bouncing rays: calculating the RCS of an arbitrarily shaped cavity, IEEE Trans. Antennas Propagat., 37 (1989), 194–205.
[13] J. Liu and J. Jin, A special higher order finite-element method for scattering by deep cavities, IEEE Trans. Antennas Propagat., 48 (2000), 694–703.
[14] P. Monk, Finite Element Methods for Maxwell's Equation, Oxford University Press, 2003.
[15] H. Mosallaei and Y. Rahmat-Samii, RCS reduction of canonical targets isomg genetic algorithm synthesized RAM, IEEE Trans. Antennas Propagat., 48 (2000), 1594–1606.
[16] J. Nocedal and S. J. Wright. Numerical Optimization, Second Edition, Springer Series in Operations Research, Springer Verlag, 2006.
[17] S. Ohnuki and T. Hinata, RCS of material partially loaded parallel-plate waveguide cavities, IEEE Trans. Antennas Propagat., 51 (2003), 337–344.
[18] W. Sun and J. M. Wu, Newton-Cotes formulae for the numerical evaluation of certain hypersingular integral, Computing, 75 (2005), 297–309.